Journal of Inflammation Research

Dovepress
Taylor & Francis Group

Open Access Full Text Article

ORIGINAL RESEARCH

SIRT2 Promotes NLRP3-Mediated Microglia Pyroptosis and Neuroinflammation via FOXO3a Pathway After Subarachnoid Hemorrhage

Jia-Qing Sun[1,5,*], Bin Sheng[2,5,*], Sen Gao[2,5,*], Xun-Zhi Liu[2,5], Yue Cui[4,5], Zheng Peng[2,5], Xiang-Xin Chen[2,5], Peng-Fei Ding[3,5], Zong Zhuang[2,5], Ling-Yun Wu[2,5], Chun-Hua Hang[1–5], Wei Li[2–5]

[1]Department of Neurosurgery, Nanjing Drum Tower Hospital, Drum Tower Hospital Clinical College, Xuzhou Medical University, Nanjing, People's Republic of China; [2]Department of Neurosurgery, Nanjing Drum Tower Hospital, Affiliated Hospital of Medical School, Nanjing University, Nanjing, People's Republic of China; [3]Department of Neurosurgery, Nanjing Drum Tower Hospital Clinical College of Nanjing Medical University, Nanjing, People's Republic of China; [4]Department of Neurosurgery, Nanjing Drum Tower Hospital Clinical College of Nanjing University of Chinese Medicine, Nanjing, People's Republic of China; [5]Neurosurgery Institute of Nanjing University, Nanjing, People's Republic of China

*These authors contributed equally to this work

Correspondence: Chun-Hua Hang; Zong Zhuang, Department of Neurosurgery, Nanjing Drum Tower Hospital, The Affiliated Hospital of Nanjing University Medical School, Nanjing, 210006, People's Republic of China, Tel +86 25 83106666-11902; +86 25 83106666-11901, Email hang_neurosurgery@163.com; zhuangzong@njglyy.com

Purpose: This study primarily elucidating the specific mechanism of SIRT2 on neuroinflammation and microglial pyroptosis in a mouse model of SAH.

Patients and Methods: CSF were collected from 57 SAH patients and 11 healthy individuals. C57BL/6 mouse SAH model was established using prechiasmatic cistern blood injection and the in vitro hemoglobin (Hb) stimulation microglia model. Lentivirus was used as a vector for RNA interference technology to knock down the SIRT2 gene expression. Small interfering RNA was used to knockdown the expression of FOXO3a. The tools included measurements of brain water content, neurological scores, Western blot, PCR, ELISA, TEM, immunofluorescence, LDH assay, modified Garcia score, and balance beam tests to evaluate changes in pyroptosis and neuroinflammatory responses.

Results: In CSF samples from SAH patients, elevated levels of SIRT2 and GSDMD were observed, with SIRT2 demonstrating particular diagnostic value for predicting prognosis at the 3-month follow-up. SIRT2 upregulation exacerbated neurological deficits, brain edema, and blood-brain barrier disruption in mice following SAH. SIRT2 increased GSDMD, caspase-1, and IL-1β/IL-18 expression, and amplified GSDMD-positive microglia. FOXO3a was also upregulated post-SAH. siRNA-mediated SIRT2 knockdown ameliorated microglial pyroptosis after SAH. FOXO3a siRNA reduced NLRP3 inflammasome activation and microglial pyroptosis severity, along with neuroinflammation post-SAH.

Conclusion: In summary, SIRT2 promoted microglial pyroptosis, primarily by increasing the expression and activity of Foxo3a, thereby exacerbating neuroinflammatory damage following subarachnoid hemorrhage.

Keywords: SIRT2, subarachnoid hemorrhage, FOXO3a, GSDMD, microglial pyroptosis

Introduction

Subarachnoid hemorrhage (SAH) is a devastating cerebrovascular disease, accounting for approximately 3.1% of all stroke subtypes, with a short-term mortality rate up to 19% and a very high recurrence rate.[1] Despite significant advances in neurosurgery, reversing the high mortality and disability rates caused by SAH remains impossible, imposing a substantial economic burden on families and society.[2] Research shows that early brain injury (EBI) plays a key role in SAH, triggering a series of complex pathophysiological processes including oxidative stress, inflammatory response, mitochondrial dysfunction and pyroptosis. The interaction between these processes leads to irreversible neural cell loss and brain tissue damage, affecting both the short-term and long-term clinical prognosis of patients.[3] Among these

Received: 2 August 2024
Accepted: 14 December 2024
Published: 27 December 2024

processes, neuroinflammatory reaction predominates in the pathophysiological processes following SAH.[4] Microglia, the resident immune cells in brain tissue, become activated following SAH, inducing the release of numerous pro-inflammatory factors, thereby exacerbating the neuroinflammatory response.[5,6]

Recent research demonstrates that pyroptosis is a specific type of programmed cell death closely related to inflammation. It is morphologically similar to necrosis but distinct from apoptosis. It plays a crucial role in inflammation-related diseases.[7,8] Microglial pyroptosis has become a target for therapeutic breakthroughs in various nervous system-related diseases and plays a crucial role in the prognosis of brain injury, neurodegeneration and cerebrovascular diseases.[9–11] Additionally, evidence indicates that microglial pyroptosis plays a significant role in the pathological process of neuroinflammation and secondary neurological damage following SAH.[12,13] The inflammasome typically serves as the initiating factor for cell pyroptosis following SAH. Upon activation, it recruits and activates caspase-1, cleaves Gasdermin family members (GSDMD), and generates the active amino-terminal (GSDMD-N), which attaches to the cell membrane to form pores. This process leads to cell swelling, lysis, and release of pro-inflammatory cytokines such as interleukin 1β (IL-1β) and interleukin 18 (IL-18), triggering a potent neuroinflammatory response and causing significant damage to neural tissues.[14,15] The inflammasome is a large multiprotein complex situated in the cytoplasm, which detects and reacts to pathogen associated molecular patterns (PAMPs) or damage-associated molecular patterns (DAMPs) within cells. Different types of inflammasomes have been identified, including NLRP1, NLRP3, NLRC4, IPAF, and AIM2. Among them, the NLRP3 inflammasome is the most extensively studied and crucial, with its activation involving multiple signaling pathways.[16,17] Sufficient research evidence demonstrates that regulating the NLRP3 inflammasome and GSDMD-mediated pyroptosis can markedly ameliorate neurological dysfunction following SAH, leading to reduced mortality and disability rates among SAH patients.[18] In recent years, microglial pyroptosis has garnered considerable scholarly attention due to its pivotal role in the pathological progression following stroke.[10,19,20] Nonetheless, its precise mechanism remains incompletely understood, particularly in the context of SAH, with relatively few studies investigating this mechanism.[21] Hence, our targeted inhibition of pyroptosis following microglial activation and successive neuroinflammation may represent an effective therapeutic approach to mitigate dysfunction and damage following SAH.

SIRT2, also known as Sirtuin 2, is a member of the Sirtuin family and is classified as an atypical deacetylase.[22] SIRT2 plays a critical role in various biological processes, including cellular metabolism, cell cycle regulation, DNA repair, and inflammatory responses, primarily through the deacetylation of multiple substrate proteins in the nucleus and cytoplasm.[23] Research has highlighted SIRT2's pivotal role in regulating several diseases, including neurodegenerative disorders, tumors, and metabolic diseases, although its mechanisms may exhibit dual roles. For instance, while some studies have associated high SIRT2 expression with stroke and the progression of neurodegenerative diseases.[24–26] While other research has reported contrary findings.[27] This discrepancy could be due to SIRT2's involvement in neuroinflammation and oxidative stress. Previous studies have shown that SIRT2 is crucial for the activation of microglia and brain injury in neuroinflammation models.[28] Additionally, inhibiting SIRT2 has been shown to confer neuroprotection post-ischemic stroke.[29] In traumatic brain injury studies, SIRT2 inhibition reduced the expression of NLRP3 inflammasomes and decreased caspase-1 activation, leading to lower pyroptosis and reduced neuroinflammation.[30] Therefore, SIRT2 inhibition might offer a novel approach for treating neuroinflammatory diseases. However, the potential of SIRT2 inhibition to mitigate neuroinflammation and cell death following SAH remains unexplored. Forkhead box O3a (FOXO3a), a key member of the forkhead box transcription factor family, is a significant target for SIRT2-mediated deacetylation.[31]

Inhibiting SIRT2 has been shown to decrease FOXO3a levels and prevent its nuclear translocation, reducing cell pyroptosis and preserving neurological function post-ischemic stroke.[25] Additionally, FOXO3a plays a key role in pyroptosis, as evidenced by studies showing that in liver cancer, metformin can significantly upregulate FOXO3a levels, further activating NLRP3 to induce apoptosis and pyroptosis.[32] The levels of FOXO3a are positively correlated with the severity of traumatic brain injury and are involved in neurological damage and inflammatory responses following brain hemorrhage.[33,34] However, the involvement of FOXO3a in microglial pyroptosis and neuroinflammation following SAH is largely unknown.

Currently, no studies have explored the relationship between SIRT2 and NLRP3 in SAH. Since post-SAH neuroinflammation and poor prognosis are associated with the activation of the NLRP3 multiprotein complex, research in this

field is still in its preliminary stages. Therefore, further experimental and clinical studies are necessary to elucidate the exact role and mechanism of SIRT2 and NLRP3-regulated microglial pyroptosis in the pathophysiology of SAH, to facilitate substantial progress in the treatment strategies for SAH patients.

Methods and Materials

Experimental Program

The animal experiments were described in Figure 1.

Experiment 1

Assessment of temporal expression changes of SIRT2, GSDMD/GSDMD-N, NLRP3 following SAH.

Animals were randomly divided into six groups (Sham, 6h, 12h, 24h, 48h, and 72h post-SAH, n=8-10 per group). The SAH model was induced, and mice were euthanized at the specified time points (6h, 12h, 24h, 48h, and 72h post-SAH). Six mice from each group were selected for Western Blot and PCR analyses, while the remaining were subjected to immunofluorescence staining analysis.

Experiment 2

Assessment of the effect of SIRT2 on neurological function in mice after SAH.

Animals were randomly divided into four groups (Sham, SAH, Si-SIRT2+Sham, and Si-SIRT2+SAH, n=14-16 per group), injected with Si-RNA-SIRT2 intracerebroventricularly (*iv*) 72h before SAH. Neurological function scores, balance beam tests, cerebral edema measurements, and SAH grading were conducted at 24h post-SAH. And the expression of tight junction proteins were evaluated by Western Blot.

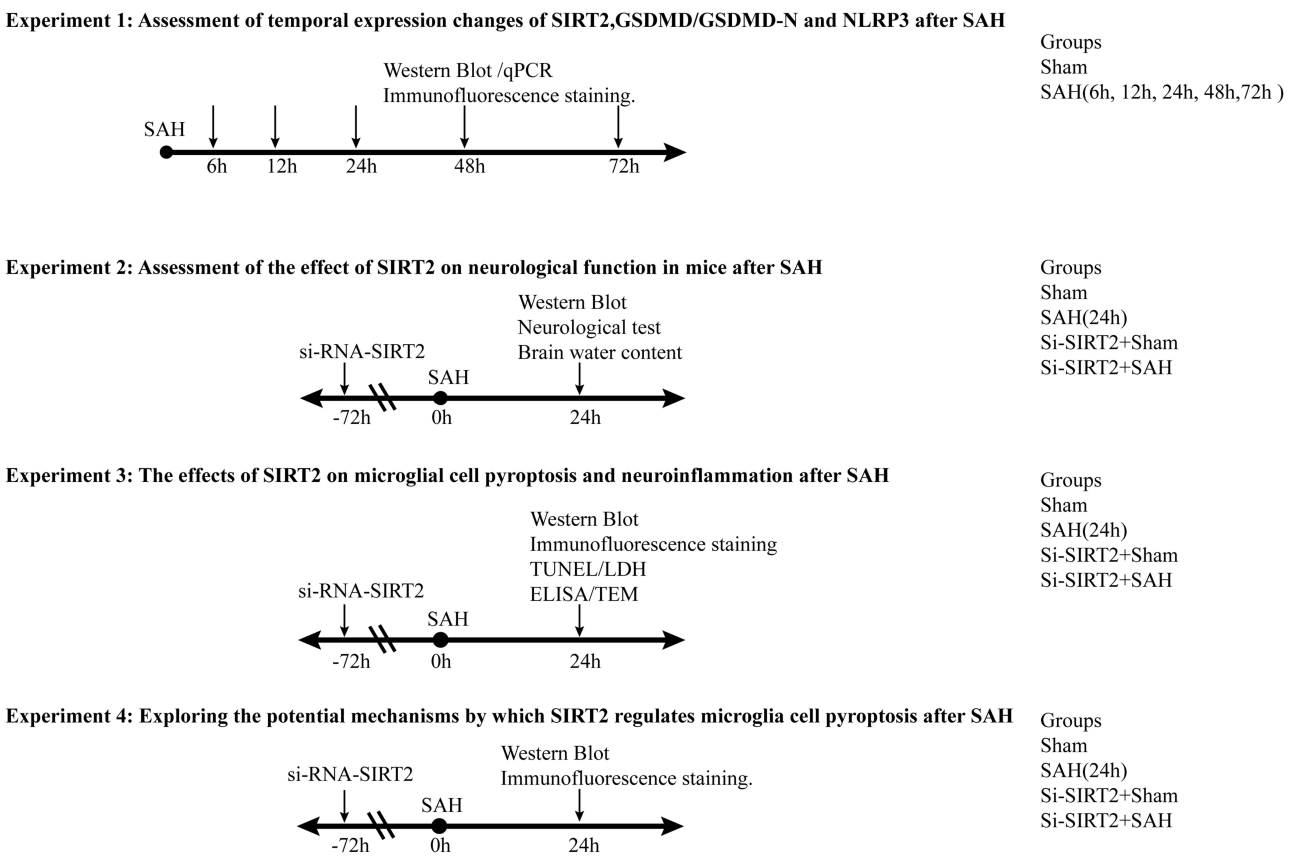

Figure 1 Animal experimental design and groups.

https://doi.org/10.2147/JIR.S487716

Experiment 3

Exploring the critical role of SIRT2 in microglia pyroptosis after SAH.

Si-RNA-SIRT2 was injected intracerebroventricularly 72 hours before inducing SAH. The subjects were divided into four groups: Sham, SAH, Si-SIRT2+Sham, and Si-SIRT2+SAH, with 15–20 subjects in each group. The efficacy of pyroptosis indices, neuroinflammation and knockdown efficiency was verified using Western Blot, immunofluorescence staining, TUNEL assay, ELISA, LDH assay and TME.

Experiment 4

Exploring the potential mechanisms of SIRT2-mediated microglial pyroptosis following SAH.

Animals were randomly divided into four groups (Sham, SAH, Si-SIRT2+Sham, and Si-SIRT2+SAH, n=15-20 per group). Research methods included Western Blot and immunofluorescence staining.

Cerebrospinal Fluid Patient Recruitment and Sample Preparation

The experimental design was approved by the Ethics Committee of Nanjing Drum Tower Hospital, Affiliated Hospital of Medical School, Nanjing University and informed consent forms were signed by all participating patients (approval number: No. 2022–294). This study involved 57 patients admitted to the hospital within three days of SAH onset, serving as the experimental group, and cerebrospinal fluid (CSF) from 11 healthy individuals as the control group. The clinical characteristics of SAH patients and healthy volunteers have been detailed in Table 1. Each specimen was measured three times, and the averages were calculated. Patients were considered for inclusion in the study if they satisfied the following conditions: 1) The patient or a legally authorized representative voluntarily provided written informed consent for participation in the trial; 2) They were diagnosed with SAH due to a ruptured intracranial aneurysm and had undergone interventional surgical treatment within a 72-hour time window; 3) Age between 20 and 70 years; 4) For the control group, inclusion was limited to individuals aged 20 to 70 years, comprising either patients scheduled for cesarean section or volunteers without any neurological conditions requiring spinal anesthesia. Individuals were excluded from the study on the basis of the following: 1) Failure to fulfill the aforementioned inclusion criteria; 2) Presence of a large intracranial hematoma; 3) Evidence of severe cardiac, hepatic, renal, or hematological disorders; 4) Diagnosis of intracranial tumors. The collected CSF samples were immediately centrifuged at 4°C and 3000 rpm for 10 minutes and subsequently stored at −80°C for further analysis. The expression levels of SIRT2 in the samples were measured following the ELISA kit manufacturer's instructions. All SAH patients received standard care and had clinical information collected, including age, gender, and medical history. Prognosis was assessed using the Hunt-Hess score at admission and the modified Rankin Scale (mRS) score 6 months post-discharge. Patients with mRS scores <3 were classified as favorable prognosis group, while those with mRS scores ≥3 were classified as the poor prognosis group.[35]

Animals and SAH Models

The necessary male C57BL/6J mice (weighing 25–30g and aged 6–8 weeks) were supplied by the Animal Center of Nanjing Drum Tower Hospital, Affiliated Hospital of Medical School, Nanjing University. All animal study protocols received approval from the Animal Experimental Ethics Committee of Nanjing Drum Tower Hospital and strictly adhere to the "Guide for the Care and Use of Laboratory Animals" issued by the National Institutes of Health in the United

Table 1 Clinical Characteristics of SAH and Healthy Participants Samples

Variables	Total	SAH	Without SAH	*P* value
Samples(n)	68	57	11	
Genders(n)				
Male	33	29	4	0.71
Female	35	28	7	
Ages (years)	50.0±1.1	50.1±1.2	49.9±3.9	0.07

States. All experimental mice were housed under temperature 25°C approximately and humidity-controlled conditions, with free access to food and water. As described in our previous studies, the prechiasmatic cistern SAH model was employed.[36] In brief, the mice were anesthetized with 2% isoflurane (2% oxygen, 300 mL/min) and positioned in a stereotactic frame. Following disinfection, a midline scalp incision approximately 1.0 cm in length was made to expose the skull. A 1.0 mm diameter hole was drilled 4.5 mm anterior to the bregma along the midline. Subsequently, a donor mouse was euthanized by cardiac puncture to obtain arterial blood. Next, 50μL of arterial blood was injected into the prechiasmatic cistern via the pre-drilled hole. The needle was maintained in place for 1–2 minutes during the injection to prevent blood reflux and ensure successful modeling. For the sham group, the same surgical procedure was performed, but an equivalent volume of saline solution was injected. Finally, the scalp was sutured, and following stabilization, the mice were returned to their cages. Neurological function was assessed 24 hours later using a modified Garcia score, with mice scoring ≤6 or ≥15 being excluded.

SiRNA-SIRT2 Infection in vivo

Following induction of anesthesia using isoflurane, the mice were placed in a stereotactic frame. A 10 μL Hamilton syringe was used to insert a needle into the left lateral ventricle through a drilled hole, using coordinates of 1.0 mm posterior to the bregma, 1.5 mm lateral to the midline, and 3.2 mm below the dura. According to the manufacturer's instructions and siRNA efficacy assessment, SIRT2 siRNA (siB14529151009-1-5, Ribobio) was administered at a rate of 0.5 μL/min into the left lateral ventricle two days prior to SAH induction. After completing the injection, the scalp was sutured, and the mice were returned to their cages for regular housing.

Cellular and in vitro Model Culture

To culture primary microglia, neonatal mouse brains must be collected within 24 hours of birth. After removing the meninges under a microscope, the brain tissue is carefully excised, placed on ice in a petri dish, and cut into approximately $1mm^3$ pieces, which are then placed into pre-warmed TrypLE (#12563029, Gibco, Suzhou, China). The tissue is digested for 10 minutes in a 37°C incubator. The digestion is then halted by adding 2 mL FBS, and the collected cells are transferred to culture flasks. We cultured primary microglia in high glucose medium (DMEM, #C11995500BT, Gibco, Suzhou) supplemented with 10% fetal bovine serum (FBS, #10099141C, Gibco, Australia) and 1% penicillin-streptomycin (#10378016, Gibco, Suzhou). The medium was changed on days 3 and 7. On days 10 and 13, the culture flasks were gently shaken to collect suspended microglia, which were then transferred to well plates for further experiments. BV2 (#ZQ0397, Shanghai, China) is a clonal microglial cell line. We cultured BV2 in DMEM supplemented with 10% FBS and 1% penicillin-streptomycin, and incubated them at 37°C.[37] The medium was changed and the cells were passaged every other day. To mimic the SAH in vitro model, BV2 and primary microglia were typically stimulated with 25 μmol/L Hb.

Brain Edema Measurement

Assessment of the degree of brain edema in mice was performed by the wet-dry method; briefly, mice were executed within 24 hours of modeling and the wet weight of their brain tissue was measured, followed by drying the samples in an oven at 100°C for 24 hours, removing them and measuring their dry weight. Brain water content was calculated as [(wet weight - dry weight)/wet weight] × 100%.

Behavioral Assessment

Twenty-four hours post-SAH, short-term neurological function was evaluated using the Modified Garcia Score and the Balance Beam Experiment. The Modified Garcia Score assesses six domains: voluntary movement, postural symmetry, forelimb extension, climbing ability, bilateral body tactile responses, and bilateral whisker tactile responses. Each domain was scored on a scale from 0 to 3, yielding a total score between 3 and 18, where a higher score indicates less severe neurological impairment. The Balance Beam Experiment measures motor coordination and balance. Each mouse underwent the test three times, and the average score was recorded. The scoring criteria are as follows: 0, the mouse cannot grasp or falls immediately; 1, the mouse can grasp or sit but does not move, remaining for 1 minute; 2, the mouse can

move but falls within 1 minute; 3, the mouse can walk from one end of the beam to the other but is prone to falling; and 4, the mouse moves freely across the beam.

Nucleocytoplasmic Fractionation

We employed the Nuclear and Cytoplasmic Protein Extraction Kit (#P0028, Beyotime, Nanjing) to isolate nuclear and cytoplasmic proteins. Cytoplasmic Protein Extraction Reagents A and B were sequentially added to the collected cell pellets, following the manufacturer's instructions. The cytoplasmic proteins were then extracted by vigorous vortexing and centrifugation at 12,000–16,000g for 5 minutes at 4°C, with the supernatant transferred to a new EP tube. The nucleus extraction reagent was subsequently added to the remaining pellet to isolate nuclear proteins, repeating the same steps as for cytoplasmic proteins.

Immunofluorescence Staining (IF)

Intact mouse brain tissues were fixed in 4% paraformaldehyde (#P0099, Beyotime, NJ) for 24 hours and dehydrated using a gradient of 15% and 30% sucrose. Frozen sections of 10 μm thickness were blocked with 1% milk protein for 1 hour at room temperature, followed by overnight incubation at 4°C with the primary antibody. After three washes with phosphate buffer solution (PBS), the sections were incubated with the corresponding fluorescent secondary antibody for 2 hours at room temperature and then rinsed three times with PBS. The sections were finally sealed with a fluorescence quencher containing DAPI (#D21490, Thermo). Immunofluorescence staining of microglia involved cell inoculation into well plates, followed by fixation, permeabilization, blocking, and antibody incubation, concluding with sealing. Fluorescence images were captured using the Leica Thunder fluorescence microscope system, Olympus FV3000, and Nikon A1R MP confocal microscope system. Post-analysis was conducted using ImageJ, Olympus CellSens software, and NIS-Elements Viewer software.

Tunel

Double immunostaining for NeuN and terminal deoxynucleotidyl transferase dUTP nick end labeling (TUNEL) was performed 24 hours post-SAH using a TUNEL staining kit (#C1086, Beyotime, Nanjing) according to the manufacturer's protocol. Cells were incubated in TUNEL assay solution at room temperature for 1 hour under light protection, followed by sealing with a fluorescence quencher containing DAPI. Cell morphology was then observed at 480 nm using a fluorescence microscope.

Western Blot (WB)

Brain tissues and cell samples were lysed using RIPA buffer (#P10013B, Beyotime, Shanghai) containing phosphatase inhibitor (#GRF102, Epizyme, Shanghai) and protease inhibitor (#GRF101, Epizyme, Shanghai), and protein concentrations were quantified using the BCA Protein Assay Kit (#P0012S, Beyotime, Nanjing). For Western Blot, equal amounts of protein were loaded into PAGE gel wells for separation, and the proteins were transferred onto polyvinylidene difluoride (PVDF, #1620177, 1620264, Millipore) membranes. The membranes were blocked for 2 hours at room temperature with 5% skimmed milk, washed three times with Tris-buffered saline with Tween 20 (TBST, #PS103, Yase, Shanghai), and then incubated overnight at 4°C with the primary antibody. The next day, the membrane was washed three times with TBST, and the corresponding secondary antibody was added and incubated for 2 hours at room temperature. The bands were analyzed using the Fiji 2.0 gel tool. The antibodies involved in this experiment are shown in Table 2.

PCR

We used the RNA Isolator (#R401-01, Vazyme, Nanjing) mix to extract total RNA from collected brain tissue homogenates and cells. cDNA was synthesized using the Reverse Transcription Reagent (#R323-01, Vazyme, Nanjing) by thoroughly mixing it with the RNA extracted in the previous step. For PCR, cDNA was synthesized using SYBR Green mix (#Q331- AA, Vazyme, Nanjing) on a PCR system (Applied Biosystems, USA). GAPDH served as the internal

Table 2 Antibodies Used in the Article

Protein	Product Code	Application	Dilution Ratio	Company	Affiliating Area
SIRT2	66410-1-Ig	WB	1:2000	Proteintech	Wuhan, China
		IF	1:200		
NLRP3	68102-1-Ig	WB	1:2000	Proteintech	Wuhan, China
		IF	1:200		
GSDMD	66387-1-Ig	WB	1:2000	Proteintech	Wuhan, China
		IF	1:200		
GSDMD-N	HA721144	WB	1:500	HUABIO	Hangzhou, China
ASC(TMS1)	67,494-1-Ig	WB	1:1000		
FOXO3a	ET1604-11	WB	1:1000	HUABIO	Hangzhou, China
		IF	1:100		
ZO-1	66,452-1-Ig	WB	1:2000	Proteintech	Wuhan, China
Occludin	66378-1-Ig	WB	1:2000	Proteintech	Wuhan, China
GADPH	60004-1-Ig	WB	1:2000	Proteintech	Wuhan, China
β-Actin	66009-1-Ig	WB	1:2000	Proteintech	Wuhan, China
β-Tubulin	10094-1-AP	WB	1:2000	Proteintech	Wuhan, China

Table 3 Primers Used in the Article

Gene	Forward Primer	Reverse Primer
SIRT2	GCCTGGGTTCCCAAAAGGAG	GAGCGGAAGTCAGGGATACC
GAPDH	AGGTCGGTGTGAACGGATTTG	TGTAGACCATGTAGTTGAGGTCA

reference gene for normalization. Gene expression changes were calculated and analyzed using the $2^{-\Delta\Delta Ct}$ method. The primers used are shown in Table 3.

Lactate Dehydrogenase Assay (LDH)

To detect cytotoxicity, we used the LDH Cytotoxicity Assay Kit (#C0016, Beyotime, Shanghai, China) to measure the extent of cellular LDH release, providing a quantitative assessment of cellular damage. We followed the manufacturer's instructions to determine cytotoxicity 24 hours after SAH.

Enzyme-Linked Immunosorbent Assay (ELISA)

We employed the Human SIRT2 ELISA Kit (#ml063065-1, Mlbio, Shanghai) and the Human GSDMD ELISA Kit (#ml057626-1, Mlbio, Shanghai) to assay SIRT2 levels in human cerebrospinal fluid samples. The Mouse IL-1β ELISA Kit (#KE20021, Proteintech, Wuhan) and the Mouse IL-18 ELISA Kit (#CK-E20324, Mlbio, Shanghai) were used to detect IL-1β and IL-18 levels in homogenates of mouse brain tissues collected 24 hours after SAH. The manufacturer's instructions were strictly followed for all assays.

Transmission Electron Microscopy

When pyroptosis occurs, cells exhibit swelling, chromatin condensation, cytoplasmic protrusion, cytoplasmic vacuolization, endoplasmic reticulum expansion, and eventually, lacunae form on the cell membrane, leading to complete breakdown.[38] We used Transmission Electron Microscopy (TEM) to observe these cellular changes and assess the occurrence of microglia pyroptosis. Brain tissue was trimmed to 1 mm^3 in size. For fixation, samples were placed in electron microscope fixative (2.5% glutaraldehyde, #30092436, Sinopharm, China) for 2–4 hours at room temperature, then rinsed three times with 0.1 M PBS for 15 minutes each time, and fixed again with 1% osmium tetroxide for 2 hours, repeating the rinsing steps. Dehydration was performed using different concentrations of ethanol and acetone. For

embedding, tissues were embedded with acetone and epoxy resin embedding solution (#90,529–77-4, SPI, China) for approximately 12 hours. Curing was carried out in an oven at 60°C for 48 hours. An ultrathin slicer (#EMUC7, Leica) was used to cut sections to a thickness of about 70 nm, which were then double-stained and imaged using a TME (#TECNAI G 20 TWIN, FEI USA).

In vivo FOXO3a siRNA Transfection

The siRNA sequence targeting the mouse FOXO3a gene was designed using the Invitrogen Block-iT RNAi Designer, and after screening, the FOXO3a-small interfering RNA (siRNA) was synthesized by Jiangsu KAIJI Biotech Co., Ltd. (Sense Sequence: 5'-GGCAAGAGCUCUUGGUGGAUCAUCATT-3'; Antisense Sequence: 5'-UGAUGAUCCACCAAGAGCUCUUGCCTT -3'). The injection method was performed according to the previously described Si-SIRT2 injection method.

Statistical Analysis

All data were analyzed using mean ± standard error of the mean (SEM), with differences considered statistically significant at $p < 0.05$. Statistical analysis was performed using SPSS 25 (SPSS Inc., USA) and Prism 9 (GraphPad Software, USA). Differences between two samples were compared using Student's *t*-test, while differences among three or more groups were assessed using one-way ANOVA followed by Tukey's post hoc test.

Results

The Level of SIRT2 in CSF After SAH is Highly Correlated with the Short-Term Prognosis of Patients

To investigate the role of SIRT2 and GSDMD in SAH, ELISA tests were conducted on CSF samples from 11 healthy individuals and 57 SAH patients. Results showed markedly elevated levels of SIRT2 and GSDMD in SAH samples when compared to controls (Figure 2A and B). Analysis revealed significantly higher SIRT2 expression in patients with moderate to severe disability (mRS scores 3–6) than those with mild disability (mRS scores 0–2) (Figure 2C). Using ROC curve analysis, SIRT2 expression levels in SAH patients' CSF were found to predict short-term prognosis with an AUC of 0.8089 and significant predictive value (P=0.0002) at 3 months post-SAH (Figure 2E). However, no significant correlation was observed between SIRT2 levels and initial injury severity (Hunt-Hess 1–2 vs 3–5), possibly due to the limited sample size of healthy controls used in the study (Figure 2D).

The Expression Level of SIRT2 Increases in the Ipsilateral Cortex Following SAH and in Microglia Treated with Hb

To investigate the role of SIRT2 following SAH, we assessed its protein and mRNA expression levels in the ipsilateral cortex of mice. Western Blot analysis demonstrated a significant increase in SIRT2 expression at 24 hours post-SAH, followed by a decline (Figure 3A). PCR further confirmed elevated SIRT2 mRNA levels compared to the Sham group at the same time point (Figure 3C). Double immunofluorescence staining of Iba1 and SIRT2 revealed a notable increase in SIRT2-positive microglia 24 hours after SAH, compared to Sham (Figure 3E). To simulate the in vitro SAH model, BV2 cells and primary microglial cells were treated with hemoglobin (Hb). SIRT2 gene expression levels in Hb-stimulated BV2 cells compared to controls, peaking at 24 hours (Figure 3B and D). Immunofluorescence staining of primary microglia corroborated these findings (Figure 3F).

SIRT2 Knockdown Ameliorates Neurological Impairment, Brain Edema and Blood-Brain Barrier Disruption After SAH

To investigate the role of SIRT2 in SAH, we employed SIRT2 siRNA lentivirus to knockdown the SIRT2 gene in mice and BV2 cells. The expression of SIRT2 was markedly reduced in the lentiviral knockdown group of mice compared to the Sham group (Figure 4A), and similar results were observed in BV2 cells (Figure 4B). Western Blot analysis revealed significantly lower levels of the tight junction proteins ZO-1 and Occludin in the SAH group compared to the Sham group. Conversely, their expression was notably elevated in the Si-SIRT2+SAH group (Figure 4C and D). The modified

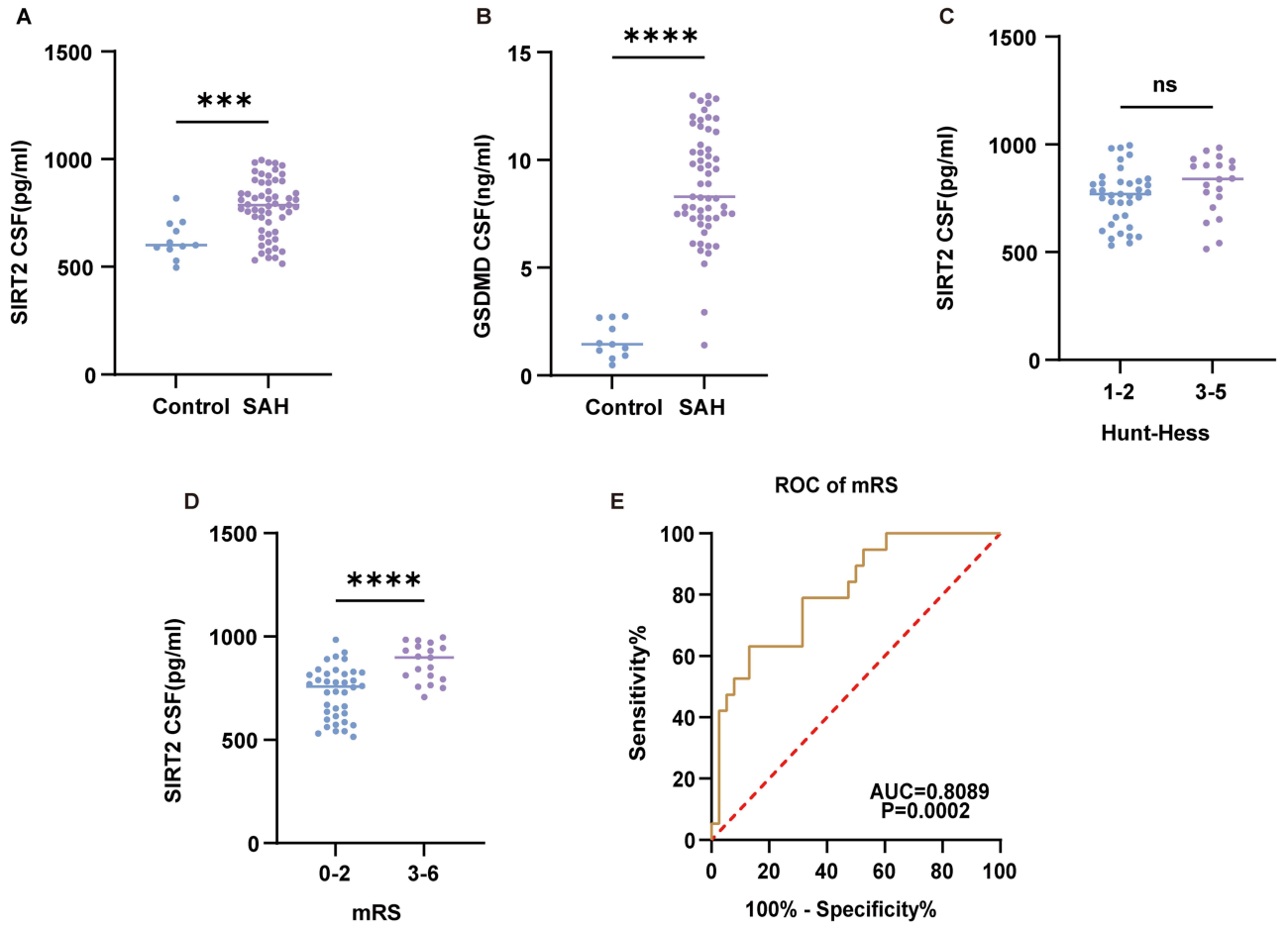

Figure 2 Expression of SIRT2 and GSDMD in human cerebrospinal fluid, and its correlation with clinical prognosis and grading of patients. (**A** and **B**) Levels of SIRT2 and GSDMD in cerebrospinal fluid of healthy individuals (n=11) and SAH patients (n=57) were detected by ELISA. (**C**) Relationship between SIRT2 expression levels and Hunt-Hess (1–2 and 3–5). (**D**) Relationship between SIRT2 expression levels and mRS (0–2 and 3–6). (**E**) ROC curves showing the predictive value of SIRT2 levels in the cerebrospinal fluid of SAH patients for 3-month prognostic follow-up. Data are expressed as mean ± SD, ns indicates not significant, ***$P < 0.001$, ****$P < 0.0001$.

Garcia and balance beam assays were employed to assess neurological impairment in mice. We observed severe neurological deficits in mice 24 hours after SAH compared to the Sham group. However, SIRT2 knockdown significantly improved neurological function scores and mitigated deficits (Figure 4E and F). Moreover, measurements of brain water content in mice indicated a significant increase after SAH, which was alleviated by SIRT2 knockdown, indicating improvement in brain edema (Figure 4G). These results suggested that knockdown of SIRT2 significantly ameliorated brain damage after SAH.

Knockdown of SIRT2 Inhibits Microglia Pyroptosis After SAH

To assess the impact of SIRT2 inhibition on microglial pyroptosis following SAH, we conducted several experiments. Western Blot analysis revealed that GSDMD and its active form, GSDMD-N, peaked 24 hours after SAH (Figure 5A). Compared to the Sham group, expression levels of GSDMD/GSDMD-N were significantly higher in the SAH group, whereas in the Si-SIRT2+SAH group, GSDMD-N levels were markedly reduced (Figure 5B). We also found that LDH release was significantly elevated after SAH and that SIRT2 knockdown reduced LDH release (Figure 5E). Immunofluorescence staining revealed increased GSDMD-positive microglia at 24 hours post-SAH, which could be attenuated by SIRT2 knockdown, and showed distinctive “ring of fire” GSDMD patterns (Figure 5G). ELISA results showed elevated levels of IL-1β and IL-18 in SAH mice compared to Sham, which were mitigated in the Si-SIRT2+SAH group (Figure 5H). The arrow in the Sham group indicates that the integrity of the microglial cell membrane is very good. In contrast, the arrow in the SAH group shows that the integrity of the microglial cell membrane is greatly

https://doi.org/10.2147/JIR.S487716

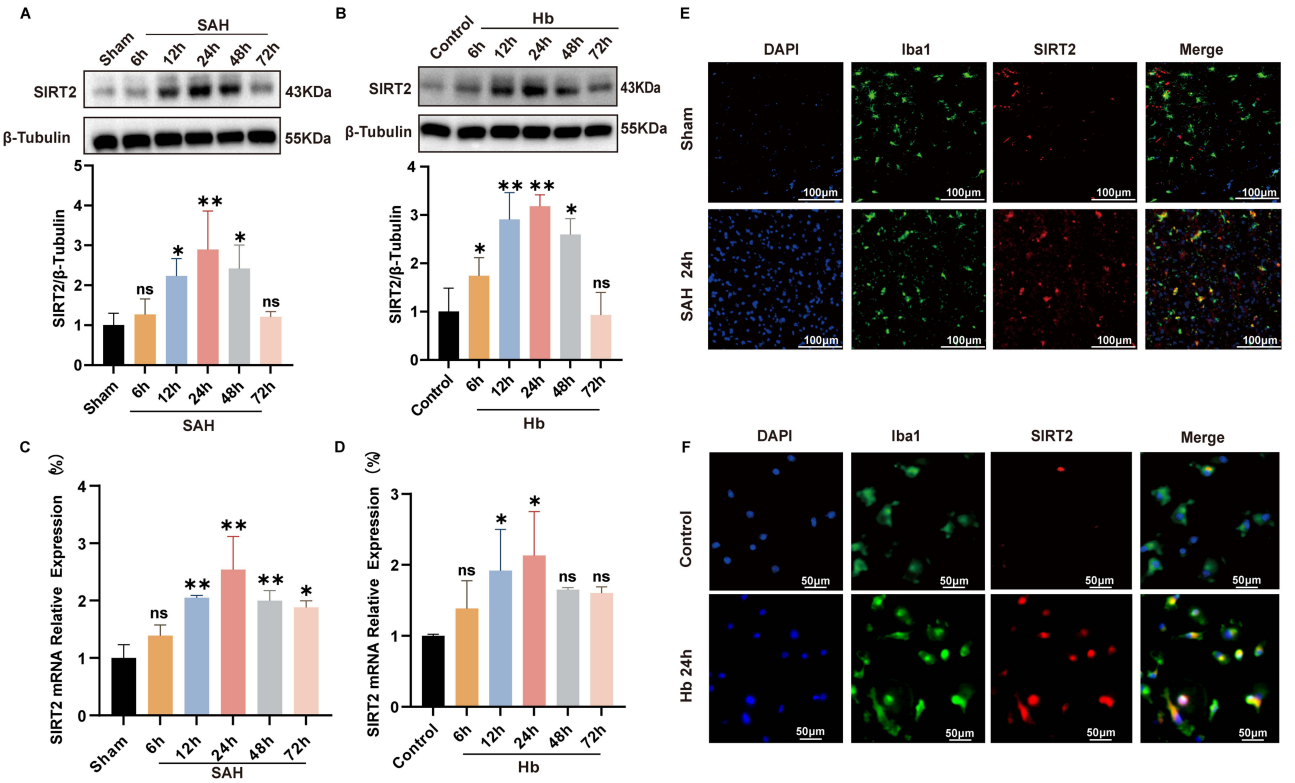

Figure 3 Changes of SIRT2 levels in vivo and in vitro models of SAH. (**A** and **B**) Protein expression changes of SIRT2 at 6h, 12h, 24h, 48h, 72h in vivo and in vitro models of SAH. (**C** and **D**) Relative mRNA expression of SIRT2 at 6h, 12h, 24h, 48h, 72h in in vivo and in vitro models after SAH detected by PCR. (**E** and **F**) Immunofluorescence co-staining of Iba1 (green) and SIRT2 (red) in microglia at 24h after SAH in vivo and in in vitro models. Data are in mean ± SD, ns indicates not significant, * $P < 0.05$, ** $P < 0.01$.

compromised. However, in the Si-SIRT2+SAH group, the cell membrane integrity, as indicated by the arrow, is significantly better than that in the SAH group. Transmission electron microscopy illustrated significantly fewer membrane pores and less membrane integrity loss in Si-SIRT2+SAH microglia compared to SAH alone (Figure 5K). TUNEL staining indicated increased Tunel-positive neurons post-SAH, which was mitigated by SIRT2 knockdown (Figure 5I).

In vitro, primary microglia and BV2 cells treated with Hb showed the same protein expression trend as in mice (Figure 5C). What is more, GSDMD/GSDMD-N with elevated expression levels after Hb stimulation was reduced by SIRT2 knockdown (Figure 5D). Immunofluorescence confirmed fewer GSDMD-positive cells and reduced CD86-positive microglia activation post-SIRT2 knockdown (Figure 5F and J). These findings collectively suggested that SIRT2 knockdown effectively inhibited microglial pyroptosis and activation following SAH.

Activation of NLRP3 is Involved in SIRT2-Mediated Microglial Cell Pyroptosis

Cellular pyroptosis, a form of cell death characterized by inflammatory vesicle activation, was investigated to determine whether NLRP3 is involved in SIRT2-induced pyroptosis of microglial cells. Western blot analysis revealed that NLRP3 expression initially increased and then decreased following SAH, with peak expression occurring at 24 hours post-SAH (Figure 6A). Additionally, we found that NLRP3 and other key proteins involved in the pyroptotic process, such as ASC and Caspase-1, were significantly higher in the Sham group 24 hours after SAH following SIRT2 knockdown in mice. This increase was mitigated in the Si-SIRT2+SAH group (Figure 6B-D). Immunofluorescence double staining of mouse brain tissue sections indicated a significant increase in NLRP3-positive microglia post-SAH, which was reversed by SIRT2 knockdown treatment (Figure 6I). Hb-stimulated BV2 cells and primary microglia were used to establish an in vitro SAH model to further validate our hypothesis. Firstly, the temporal expression pattern of NLRP3 in the in vitro model mirrored that of the in vivo experiments, with peak expression occurring at 24 hours post-intervention (Figure 6E).

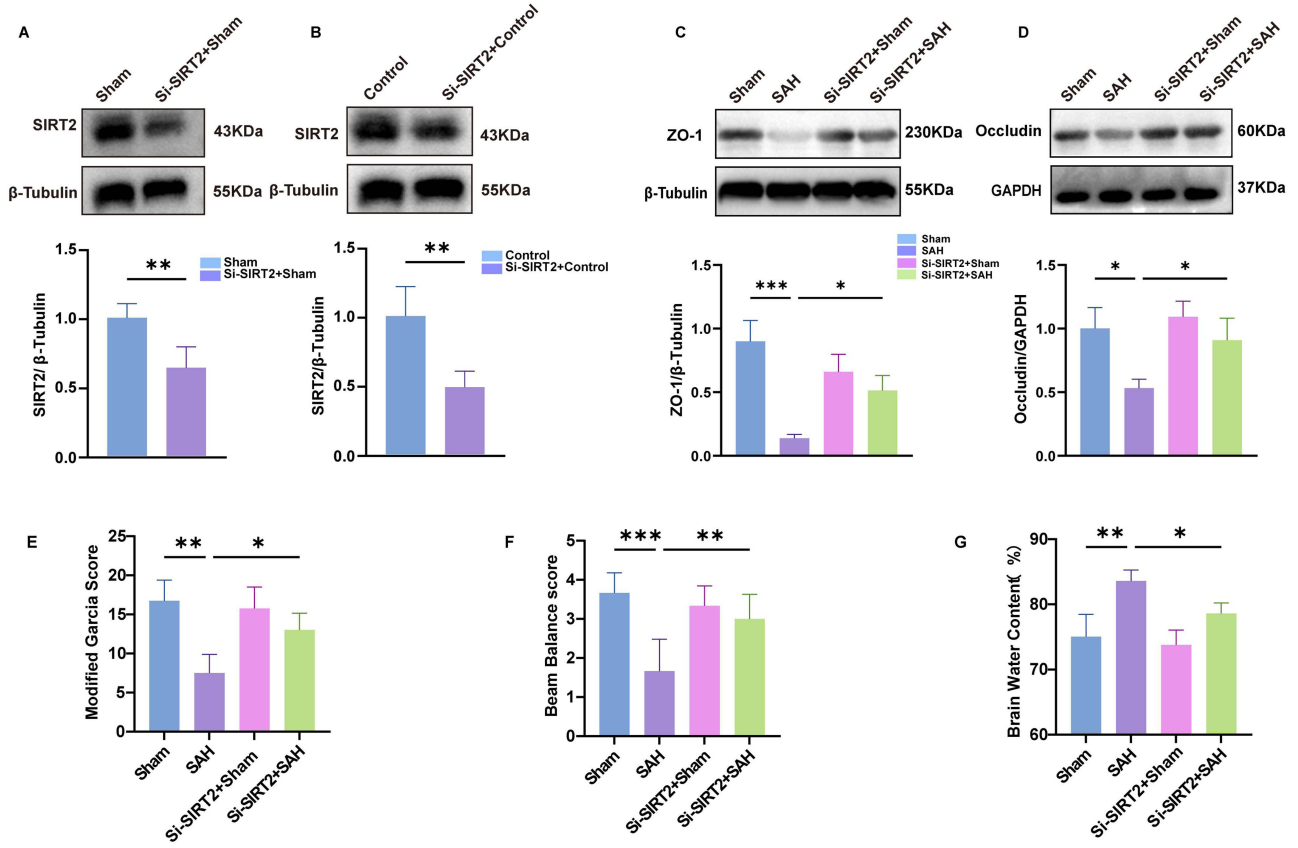

Figure 4 Knockdown of SIRT2 improves neurological function, mitigates brain edema and blood-brain barrier dysfunction. (**A** and **B**) Western blot analysis SIRT2 expression levels in vivo and in vitro following SIRT2 knockdown. (**C** and **D**) Western blot analysis illustrating alterations in expression levels of tight junctional proteins (ZO-1 and Occludin). (**E**) Modified Garcia score assessment. (**F** and **G**) Neurological function assessments (balance beam test performance and brain water content measurements). Data are in mean ± SD, * $P < 0.05$, ** $P < 0.01$, *** $P < 0.001$.

Subsequent Western blot results demonstrated significant increases in NLRP3, ASC, and Caspase-1 in microglia following Hb stimulation. The Si-SIRT2+Hb group exhibited significantly lower levels of these proteins compared to the SAH group (Figure 6F-H). Immunofluorescence staining yielded similar results to those observed in the animal experiments (Figure 6J). These findings suggested that NLRP3 played a crucial role in SIRT2-regulated microglial pyroptosis following SAH.

SIRT2 Inhibition Impedes NLRP3 Activation via FOXO3a

To elucidate whether SIRT2 activates NLRP3-mediated pyroptosis in microglial cells through FOXO3a, we observed significantly elevated levels of FOXO3a expression in post-SAH mice and Hb-treated microglial cells via Western blot analysis, and treatment with Si-SIRT2 reversed this trend (Figure 7A and B). Additionally, nucleoplasmic separation techniques revealed that FOXO3a expression was significantly reduced in the cytoplasm and increased in the nucleus after SAH compared to the Sham group. Upon SIRT2 knockdown in mice, nuclear FOXO3a levels significantly decreased post-SAH, whereas FOXO3a levels in the cytoplasm significantly increased (Figure 7C). Immunofluorescence staining demonstrated a significant increase in FOXO3a-positive staining in the nucleus post-SAH. In contrast, FOXO3a intensity in the cytoplasm was notably higher than in the nucleus after SIRT2 knockdown (Figure 7D). These findings suggested that SIRT2 activated NLRP3 following SAH by enhancing FOXO3a nuclear transcriptional activity, thus promoting its nuclear accumulation and high expression. SIRT2 knockdown effectively reversed this trend.

https://doi.org/10.2147/JIR.S487716

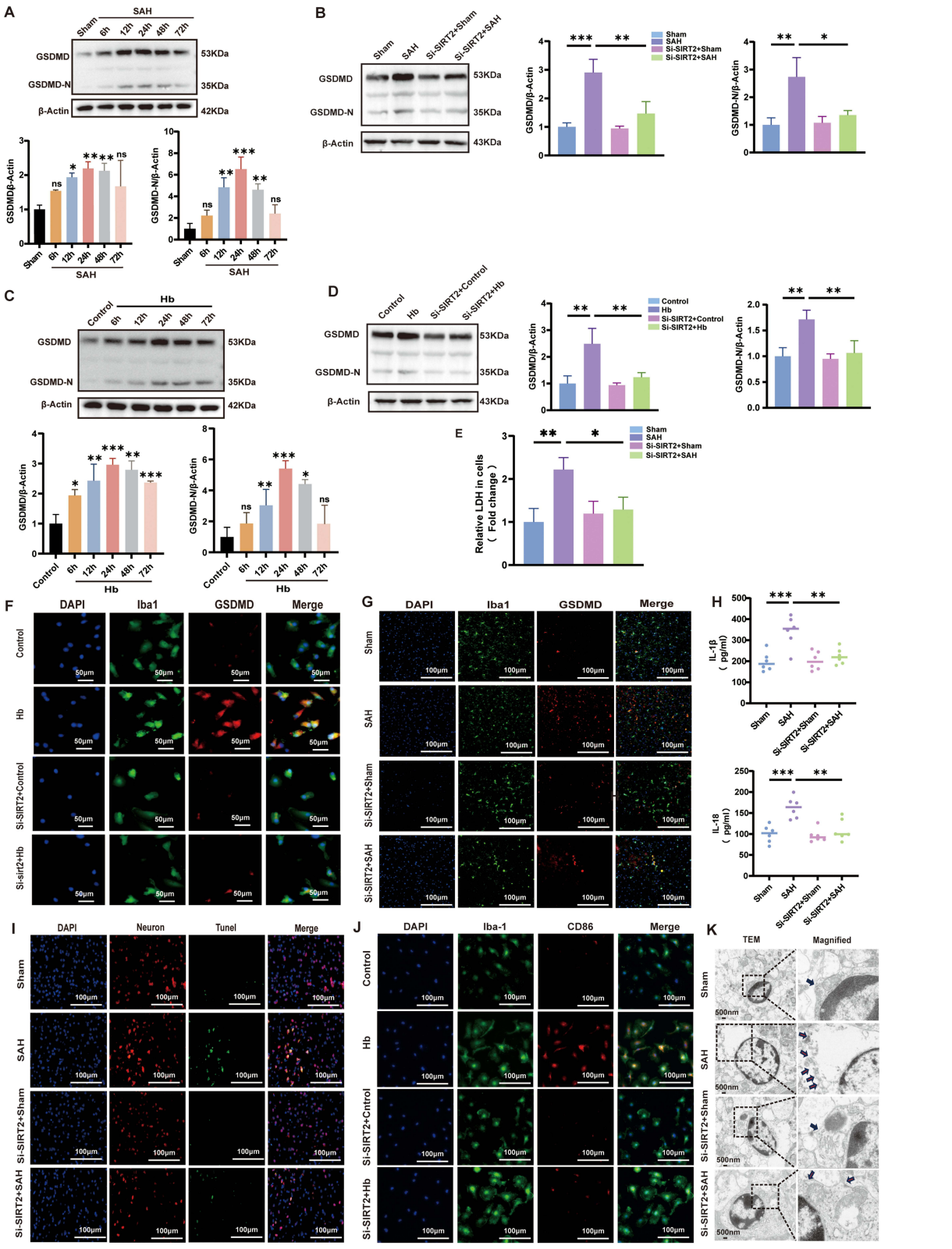

Figure 5 Knockdown of SIRT2 ameliorates microglial pyroptosis and neuroinflammation. (**A**)Western blot analysis show changes in GSDMD and GSDMD-N expression in mice at 6, 12, 24, 48, 72 hours post-SAH. (**B**) Western blot analysis GSDMD and GSDMD-N in Sham, SAH, Si-SIRT2+Sham, Si-SIRT2+SAH groups 24 hours post-SAH. (**C**) Western blot analysis changes in GSDMD and GSDMD-N temporal expression trends of proteins following Hb stimulation of microglial cells. (**D**) Western blot analysis GSDMD and GSDMD-N in microglia after 24 hours of Hb stimulation in each group. (**E**) LDH assay used to measure LDH release levels in each group. (**F** and **G**) Double immunofluorescence staining for Iba-1 and GSDMD. (**H**) ELISA results show changes in IL-1β and IL-18 levels in Sham, SAH (24h), Si-SIRT2+Sham, Si-SIRT2+SAH groups. (**I**) TUNEL assay for assessing neuronal survival post-SAH. (**J**) Double immunofluorescence staining for Iba-1 and CD86 to observe microglial activation following Hb stimulation. (**K**) Transmission electron microscopy analysis to observe morphological changes in microglia pyroptosis. All arrows represents the microglial cell membrane. Data are in mean ± SD, * $P < 0.05$, ** $P < 0.01$, *** $P < 0.001$.

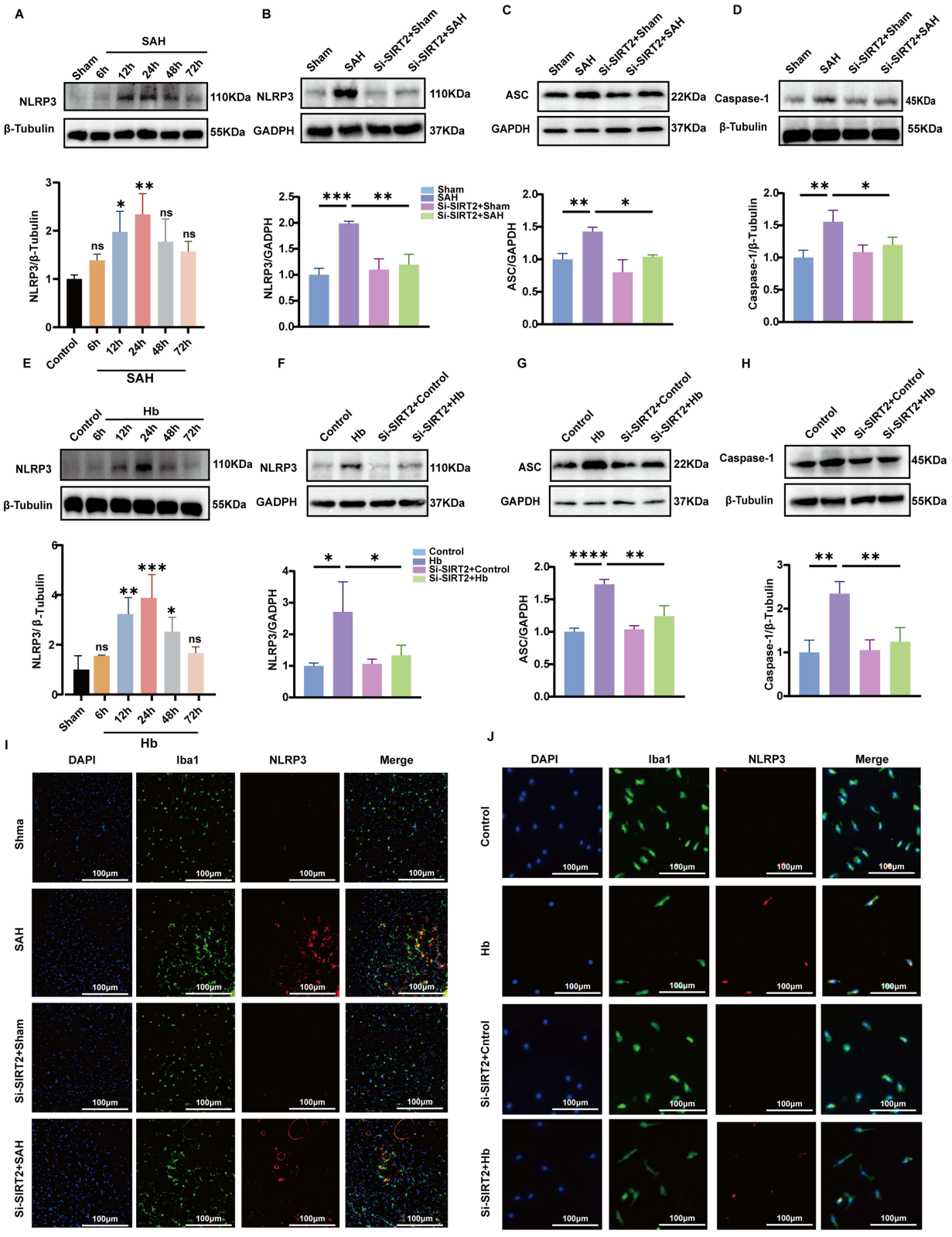

Figure 6 Knockdown of SIRT2 inhibits NLRP3 activation and microglial pyroptosis. (**A** and **E**) Western blot analysis and quantification of changes in NLRP3 protein expression levels in vivo and in vitro. (**B** and **D** and **F** and **H**) Western blot analysis and quantification of NLRP3, ASC, and caspase-1 protein expression levels in various groups in vivo and in vitro. (**I** and **J**) Double immunofluorescence staining for Iba-1 and NLRP3 in vivo and in vitro. Data are in mean ± SD, * $P < 0.05$, ** $P < 0.01$, *** $P < 0.001$, **** $P < 0.0001$.

https://doi.org/10.2147/JIR.S487716

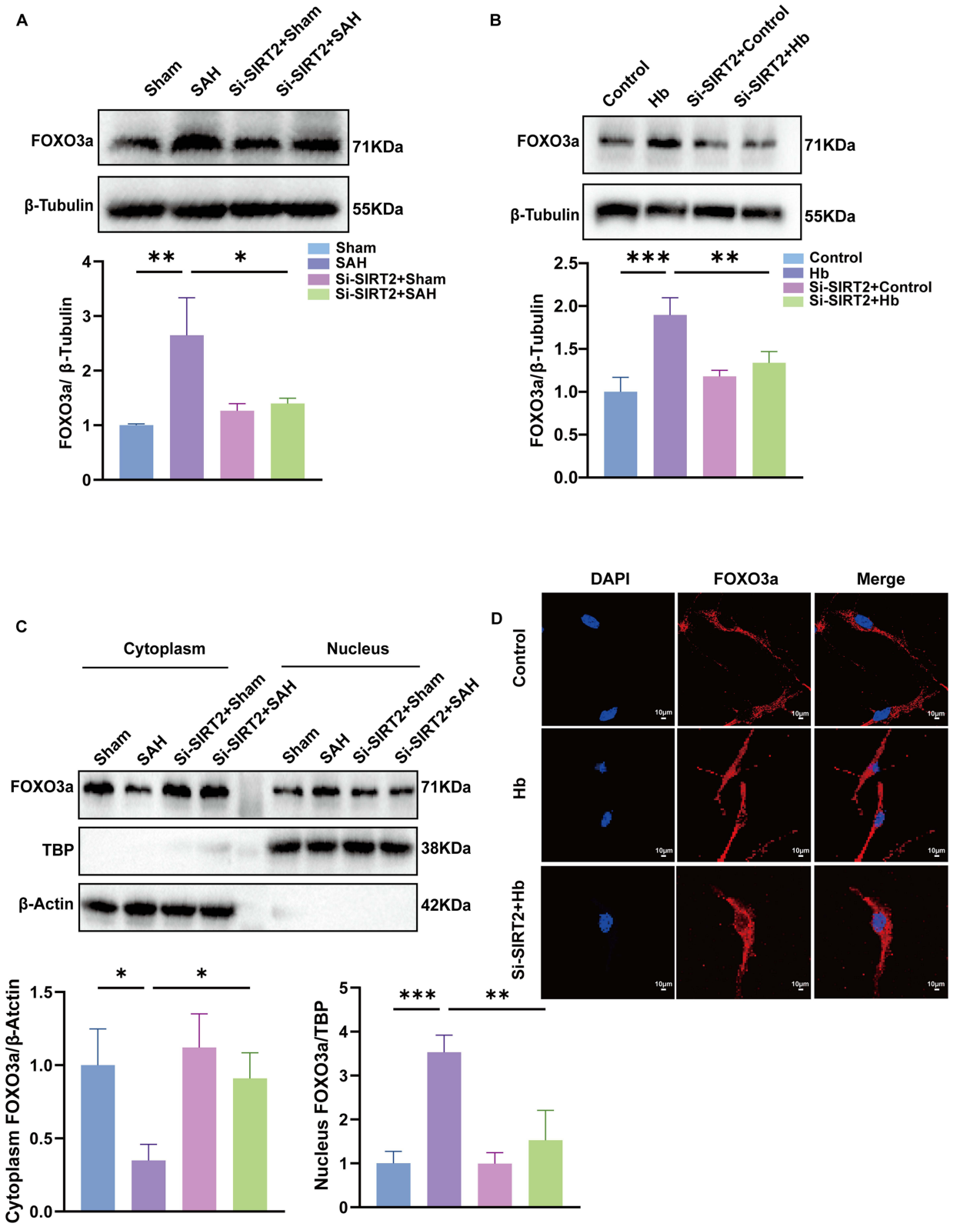

Figure 7 SIRT2 activates NLRP3 inflammasome-induced microglial pyroptosis by activating FOXO3a and promoting its nuclear localization. (**A**) Western blot analysis and quantification of FOXO3a protein expression in Sham, SAH, Si-SIRT2+Sham, and Si-SIRT2+SAH groups. (**B**) Western blot analysis and quantification of FOXO3a protein expression in Control, Hb, Si-SIRT2+Control, and Si-SIRT2+Hb groups. (**C**) Nucleoplasmic separation assay to observe the effect of siRNA knockdown of SIRT2 post-SAH on FOXO3a protein expression levels in the cytoplasm and nucleus of microglia. (**D**) Immunofluorescence analysis of FOXO3a distribution in the nucleus and cytoplasm of microglial cells. Data are in mean ± SD, * $P < 0.05$, ** $P < 0.01$, *** $P < 0.001$.

Suppression of FOXO3a Ameliorates Microglial Pyroptosis and Neuroinflammation

In this study, we aimed to investigate the role of FOXO3a in the regulation of microglial pyroptosis following SAH by SIRT2. To address this, we utilized a FOXO3a siRNA to suppress FOXO3a expression via intracerebroventricular injection in a mouse model of SAH. The effects on pyroptosis markers, including GSDMD, GSDMD-N, ASC, and caspase-1, as well as downstream inflammatory factors, were analyzed and observed.

WB analysis revealed that following SAH, the expression levels of pyroptosis-associated markers GSDMD, GSDMD-N, ASC, and caspase-1 were significantly upregulated. Notably, the administration of FOXO3a siRNA reversed this upregulation, indicating that the suppression of FOXO3a significantly ameliorated the extent of pyroptosis in SAH mice. Furthermore, the expression of neuroinflammatory factors (IL-1β) and the NLRP3 inflammasome, was also found to be inhibited upon FOXO3a suppression. Concurrently, the expression of occludin, a key protein in BBB, was significantly increased, suggesting that the inhibition of FOXO3a not only reduced the expression of inflammatory factors but also improved the disruption of the BBB post-SAH (Figure 8A-I).

To corroborate our findings, we employed immunofluorescence assays, which yielded consistent results (Figure 8J). Collectively, these data suggest that SIRT2 exacerbates microglial pyroptosis and neuroinflammation after SAH by promoting the expression of FOXO3a.

Discussion

Subarachnoid hemorrhage (SAH) is a life-threatening condition with consequences such as neuroinflammation and secondary brain damage.[39] Recent studies have identified SIRT2 as a crucial regulator after SAH, promoting neuroinflammatory responses by inducing microglial pyroptosis and activating NLRP3 inflammasomes. The present study revealed for the first time the critical role of SIRT2 involvement in the pathogenesis of SAH and provides potential directions for the development of new therapeutic strategies (Figure 9).

In this study, we initially observed that SIRT2 was upregulated following SAH and positively correlated with NLRP3 inflammasome activation and microglial pyroptosis. We demonstrated that knockdown of SIRT2 reduced the activity and expression levels of NLRP3 inflammasomes and GSDMD, thereby reversing microglial pyroptosis and neuroinflammation-induced secondary brain injury post-SAH. Further mechanistic studies revealed that SIRT2 modulated neuroinflammation and microglial pyroptosis through the Foxo3a pathway, a transcription factor known to play a key role in regulating microglial phenotype transformation and neuroinflammatory responses.[34] In the SAH model, SIRT2 enhanced the transcriptional activity of Foxo3a by promoting its nuclear translocation and upregulating the expression of its downstream inflammation-related genes, ultimately leading to neuroinflammation and pyroptosis. Additionally, this study revealed that SIRT2 knockdown modulated novel mechanisms of neuroinflammation and brain injury. Disruption of the blood-brain barrier (BBB) is a major factor in secondary neurological injury post-SAH. The integrity of the BBB relies on tight junction proteins, and its disruption leads to brain tissue edema. SIRT2 knockdown was found to attenuate the damage to tight junction proteins, reduce BBB disruption, and decrease brain tissue edema following SAH. This suggests that SIRT2 also regulates the integrity of the BBB during SAH pathology. Our clinical trial results also showed that high levels of SIRT2 in cerebrospinal fluid were significantly associated with poor prognosis in patients with SAH. Taken together, these data suggested that SIRT2 regulates microglial pyroptosis and neuroinflammatory injury post-SAH through the FOXO3a pathway.

Studies have shown that the neuroinflammatory response is crucial in the pathophysiological mechanisms following SAH, and the phenotypic transformation of microglia is an initiating factor.[6] In this study, we found that mice subjected to SAH model exhibited significant neuroinflammatory responses, and the ensuing strong immune response ultimately caused brain tissue damage. Moreover, immunofluorescence experiments revealed a significant increase in M1-positive microglia in the in vitro model post-SAH, indicating extensive microglial activation following SAH. Therefore, inhibiting the post-SAH cellular immune-inflammatory response is a crucial target for ameliorating neurological impairment. Additionally, cellular pyroptosis is an inflammatory form of programmed cell death, leading to membrane rupture, releasing numerous inflammatory factors, and inducing a strong neuroinflammatory response. Among these, caspase-1, activated by NLRP3, cleaves GSDMD to generate the active form GSDMD-N, which not only attaches to the cell membrane forming pores but also promotes the maturation of IL-1β and IL-18.[40] The same phenomenon was observed in

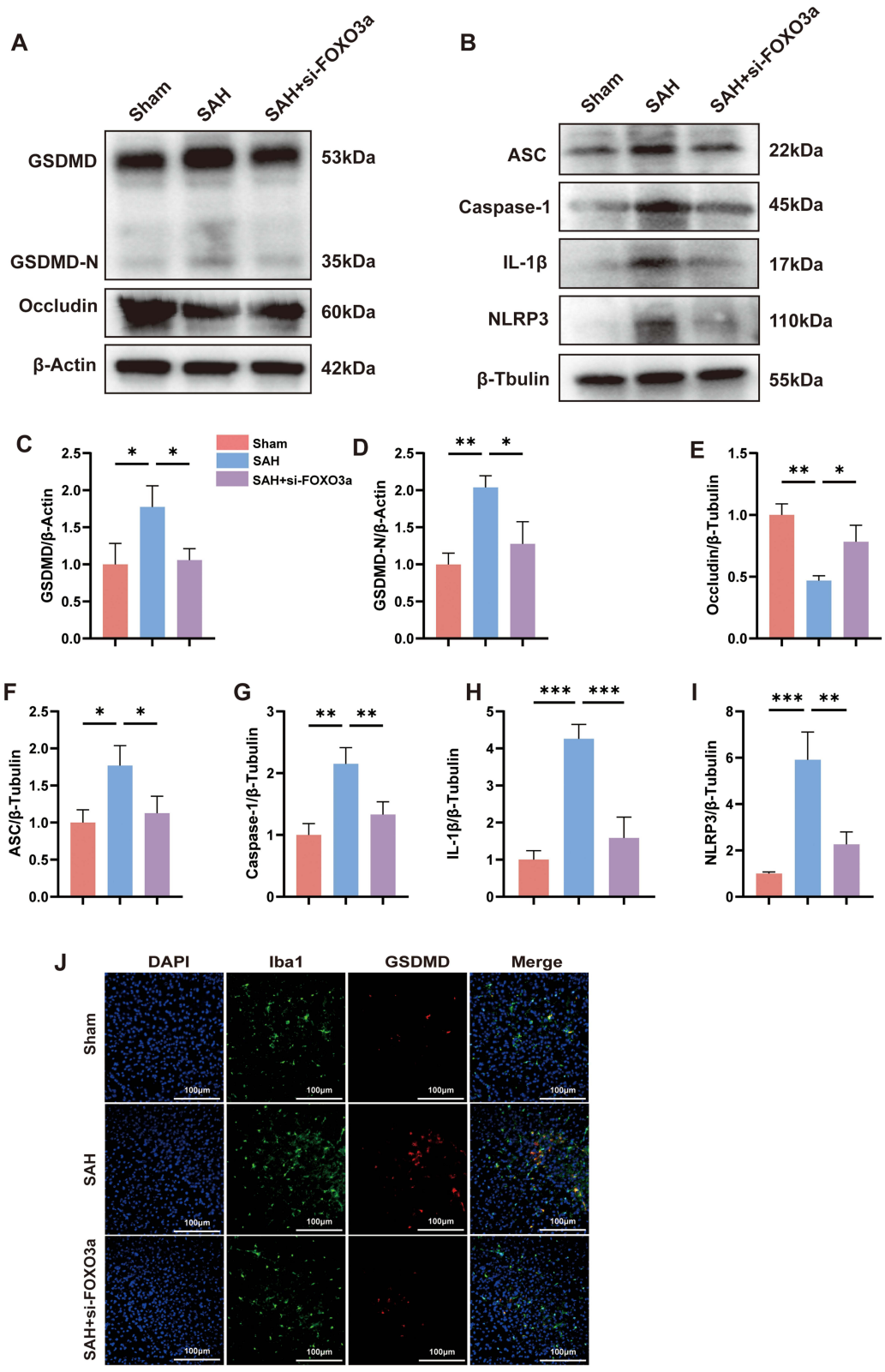

Figure 8 Suppression of FOXO3a activation and expression alleviates microglia pyroptosis and neuroinflammation following SAH. (**A**) Western blot analysis of GSDMD, GSDMD-N, and Occludin protein levels in Sham, SAH, and SAH+si-FOXO3a groups. (**B**) Expression analysis of ASC, Caspase-1, IL-1β, and NLRP3 by Western blot. (**C**) Quantitative analysis of GSDMD, (**D**) GSDMD-N, and (**E**) Occludin protein expression. (**F**) Quantitative analysis of ASC, (**G**) Caspase-1, (**H**) IL-1β, and (**I**) NLRP3 protein expression. (**J**) Immunofluorescence staining for GSDMD expression in Sham, SAH, and SAH+si-FOXO3a groups. Data are in mean ± SD, * $P < 0.05$, ** $P < 0.01$, *** $P < 0.001$.

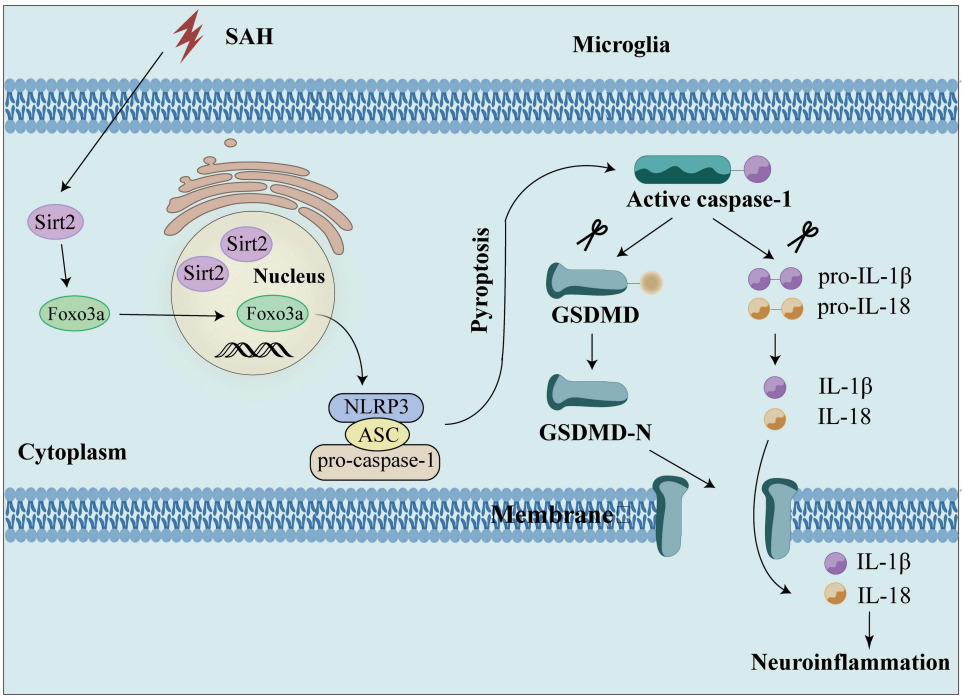

Figure 9 SIRT2 promotes GSDMD-mediated microglial pyroptosis through activation of the FOXO3a pathway following SAH. SIRT2 promotes the expression and transcription of FOXO3a after SAH, which activates NLRP3 inflammasomes and promotes caspase-1 to cleave GSDMD, resulting in the attachment of GSDMD-N to cell membrane and further perforation, which leads to the release of inflammatory mediators such as IL-1β and IL-18. Inhibition of SIRT2 attenuates microglial pyroptosis and neuroinflammation, thereby improving neurological function after SAH.

our experimental results, where GSDMD-N/GSDMD, IL-1β, and IL-18 were expressed at high levels in both SAH-modeled mice and hemoglobin-treated BV2 cells. Upon performing SIRT2 knockdown with Si-RNA in mice and BV2 cells, we found that microglial pyroptosis and neuroinflammatory factor expression were significantly reduced, suggesting that SIRT2 may regulate microglial pyroptosis post-SAH. The number of M1-type microglia and TUNEL-positive cells in SIRT2-knockdown SAH mice was also significantly lower than in normal SAH mice, indicating that inhibition of SIRT2 could reduce the conversion of microglia to a pro-inflammatory phenotype and protect neurons from damage. Moreover, SIRT2 knockdown improved neurological function, reduced brain edema, and mitigated blood-brain barrier disruption in mice. Additionally, it improved microglial pyroptosis as observed through electron microscopy, suggesting that SIRT2 knockdown can attenuate microglial pyroptosis and neuroinflammatory responses post-SAH, thus ameliorating neurological impairments.

Our results demonstrate that SIRT2 plays a crucial role in microglial pyroptosis post-SAH, and previous studies have shown SIRT2's involvement in various neurodegenerative diseases, including Alzheimer's and Parkinson's disease. However, the exact regulatory mechanism of SIRT2 on microglial pyroptosis in SAH requires further exploration. Previous studies have shown that FOXO3a can activate NLRP3's transcriptional activity to induce pyroptosis in hepatocellular carcinoma cells and various other cells, including cardiomyocytes.[32,41] Additionally, FOXO3a deficiency in microglia ameliorates brain damage after cerebral hemorrhage.[34] In order to validate our hypothesis, we strategically designed a siRNA specific to FOXO3a to selectively inhibit its expression, Our study confirmed a significant increase in the expression levels of FOXO3a and NLRP3 following SAH, and a significant increase in microglial pyroptosis, suggesting FOXO3a may be involved in regulating microglial pyroptosis post-SAH. However, the suppression of FOXO3a significantly alleviated microglial pyroptosis and downregulated the expression of neuroinflammatory factors, effectively countering the pro-inflammatory and pro-pyroptotic effects mediated by SIRT2 following SAH. This observation is in line with previous research demonstrating. Evidence suggests that the enhanced transcriptional activity of FOXO3a relies on translational modifications (eg deacetylation), and SIRT2 could deacetylate FOXO3a to promote its nuclear translocation and enhance its activity.[25,31] These cumulative findings have led us to propose that the upregulation

https://doi.org/10.2147/JIR.S487716

of SIRT2 post-SAH may intensify microglial pyroptosis and neuroinflammatory responses through the activation of FOXO3. Therefore, targeting the SIRT2-FOXO3a pathway may be an effective treatment strategy for SAH.

However, this study has some limitations. Firstly, we only focused on the role of SIRT2 in microglia. Future studies should explore the specific mechanism of SIRT2's action in neurons and other cells. Secondly, we further elucidated the role of FOXO3a in microglial pyroptosis post-SAH, suggesting that FOXO3a knockout mice and cells could be a better choice for future studies. Finally, due to limited experimental conditions, future research should employ more advanced and precise techniques to provide stronger evidence. This study provides new insights into SIRT2's role in SAH. SIRT2 increases the activation of NLRP3 inflammasomes and microglial pyroptosis by regulating the FOXO3a pathway, which in turn promotes neuroinflammation. This provides important clues for developing new drugs or treatments for SAH. Future studies should further explore the specific mechanisms of SIRT2's role in neuroinflammation and brain injury, and refine the relationship between SIRT2 and NLRP3 inflammasomes. These efforts will contribute to a deeper understanding of SAH's pathological mechanisms. Ultimately, this deeper understanding not only enhances the theoretical knowledge of SAH's pathophysiology but also provides a solid foundation for developing therapies that can prevent or reduce the damage caused by SAH, leading to better patient prognoses and quality of life.

Conclusions

The level of SIRT2 increased after SAH, which activated microglial pyroptosis by promoting the nuclear transcriptional activity of FOXO3a. This study delineates SIRT2's pivotal role in SAH-induced neuroinflammation and microglial pyroptosis via the FOXO3a pathway. Our work also demonstrated for the first time that SIRT2 can regulate pyroptosis following SAH.

Abbreviations

IF, immunofluorescence staining; ELISA, enzyme-linked immunosorbent assay; TEM transmission electron microscopy; LDH, lactate dehydrogenase; WB, Western Blot; PCR, Polymerase Chain Reaction; SAH, Subarachnoid hemorrhage; Hb, hemoglobin; siRNA, small interfering RNA; EBI, early brain injury; FOXO3a, Forkhead O3a; CSF, cerebrospinal fluid; mRS, modified Rankin Scale; AUC, Area Under Curve; ROC, Receiver Operating Characteristic; BBB, the blood-brain barrier.

Data Sharing Statement

The data that support the findings of this study are available from the corresponding author upon reasonable request.

Ethics Approval and Informed Consent

This study was conducted in accordance with the ethical standards as outlined in the 1964 Declaration of Helsinki and its later amendments. Approval for this study was obtained from the Ethics Committee of Nanjing Drum Tower Hospital, Affiliated Hospital of Medical School, Nanjing University (approval number: No. 2022-294). Informed consent was obtained from all individual participants included in the study or their legal representatives.

For animal studies, All animal study protocols received approval from the Animal Experimental Ethics Committee of Nanjing Drum Tower Hospital.

Acknowledgments

We would like to express our sincere gratitude to all those who contributed to this research project. Special thanks to the members of Neurosurgery Institute of Nanjing University for their guidance and support in the experimental design and manuscript preparation. We are also grateful to the anesthesiology department of Nanjing Drum Tower Hospital for their assistance in conducting the collection of CSF in the control group. Finally, we thank Chun-hua Hang and Wei Li for their critical revision and polishing of the manuscript. This work would not have been possible without the collective effort and dedication of everyone involved.

Author Contributions

Jia-qing Sun conceived the study, participated in its design and coordination, and helped draft the manuscript. Bin Sheng carried out the animal experiments and performed data analysis. Sen Gao contributed to the study's conception and design. Xun-zhi Liu provided guidance on manuscript writing and performed statistical analysis. Yue Cui was responsible for the illustration of figures and conducted immunofluorescence staining. Zheng Peng collected clinical samples and performed enzyme-linked immunosorbent assay (ELISA). Xiang-xin Chen contributed to the interpretation of data and critically revised the manuscript for important intellectual content. Peng-fei Ding carried out transmission electron microscopy (TEM) and Western Blot (WB). Zong Zhuang and Ling-yun Wu performed lactate dehydrogenase (LDH) detection and cell experiments. Chun-Hua Hang and Wei Li revised and polished the manuscript.

All authors have made substantial contributions to the conception and design of the work, or the acquisition, analysis, or interpretation of data; have drafted the work or revised it critically for important intellectual schemcontent; have approved the version to be published; and agree to be accountable for all aspects of the work in ensuring that questions related to the accuracy or integrity of any part of the work are appropriately investigated and resolved.

Funding

This work was supported by National Natural Science Foundation of China (NSFC) (NO. 82130037 for Chun-Hua Hang, NO. 82271363 for Ling-yun Wu, NO. 81971127 for Zong Zhuang) and Nanjing Health Science and Technology Development Key Projects, China (ZKX23025 for Wei Li).

Disclosure

All authors have no personal or financial relationships that could influence the findings of this study. The authors report no conflicts of interest in this work.

References

1. Tu W-J, Wang L-D. China stroke surveillance report 2021. *Mil Med Res*. 2023;10(1):33. doi:10.1186/s40779-023-00463-x
2. Neifert SN, Chapman EK, Martini ML, et al. Aneurysmal subarachnoid hemorrhage: the last decade. *Transl Stroke Res*. 2021;12(3):428–446. doi:10.1007/s12975-020-00867-0
3. Lauzier DC, Jayaraman K, Yuan JY, et al. Early brain injury after subarachnoid hemorrhage: incidence and mechanisms. *Stroke*. 2023;54 (5):1426–1440. doi:10.1161/STROKEAHA.122.040072
4. Okada T, Suzuki H. Mechanisms of neuroinflammation and inflammatory mediators involved in brain injury following subarachnoid hemorrhage. *Histol Histopathol*. 2020;35(7):623–636. doi:10.14670/HH-18-208
5. Chen J, Wong GKC. Microglia accumulation and activation after subarachnoid hemorrhage. *Neural Regen Res*. 2021;16(8):1531–1532. doi:10.4103/1673-5374.303028
6. Chen J, Zheng ZV, Lu G, Chan WY, Zhang Y, Wong GKC. Microglia activation, classification and microglia-mediated neuroinflammatory modulators in subarachnoid hemorrhage. *Neural Regen Res*. 2022;17(7):1404–1411. doi:10.4103/1673-5374.330589
7. Kesavardhana S, Malireddi RKS, Kanneganti T-D. Caspases in cell death, inflammation, and pyroptosis. *Annu Rev Immunol*. 2020;38:567–595. doi:10.1146/annurev-immunol-073119-095439
8. Chai R, Li Y, Shui L, Ni L, Zhang A. The role of pyroptosis in inflammatory diseases. *Front Cell Dev Biol*. 2023;11:1173235. doi:10.3389/fcell.2023.1173235
9. Wu X, Wan T, Gao X, et al. Microglia pyroptosis: a candidate target for neurological diseases treatment. Review. *Front Neurosci*. 2022;2022:16. doi:10.3389/fnins.2022.922331
10. Gu L, Sun M, Li R, et al. Microglial pyroptosis: therapeutic target in secondary brain injury following intracerebral hemorrhage. *Review Front Cell Neurosci*. 2022;2022:16. doi:10.3389/fncel.2022.971469
11. Long J, Sun Y, Liu S, et al. Targeting pyroptosis as a preventive and therapeutic approach for stroke. *Cell Death Discov*. 2023;9(1):155. doi:10.1038/s41420-023-01440-y
12. Xu P, Hong Y, Xie Y, et al. TREM-1 exacerbates neuroinflammatory injury via NLRP3 inflammasome-mediated pyroptosis in experimental subarachnoid hemorrhage. *Transl Stroke Res*. 2021;12(4):643–659. doi:10.1007/s12975-020-00840-x
13. Cai W, Wu Z, Lai J, et al. LDC7559 inhibits microglial activation and GSDMD-dependent pyroptosis after subarachnoid hemorrhage. *Front Immunol*. 2023;2023:14. doi:10.3389/fimmu.2023.1117310
14. Burdette BE, Esparza AN, Zhu H, Wang S. Gasdermin D in pyroptosis. *Acta Pharm Sin B*. 2021;11(9):2768–2782. doi:10.1016/j.apsb.2021.02.006
15. Huston HC, Anderson MJ, Fink SL. Pyroptosis and the cellular consequences of gasdermin pores. *Semin Immunol*. 2023;69:101803. doi:10.1016/j.smim.2023.101803
16. Sharma D, Kanneganti T-D. The cell biology of inflammasomes: mechanisms of inflammasome activation and regulation. *J Cell Biol*. 2016;213 (6):617–629. doi:10.1083/jcb.201602089
17. Yang J, Liu Z, Xiao TS. Post-translational regulation of inflammasomes. *Cell Mol Immunol*. 2017;14(1):65–79. doi:10.1038/cmi.2016.29

18. Chen J, Li M, Liu Z, Wang Y, Xiong K. Molecular mechanisms of neuronal death in brain injury after subarachnoid hemorrhage. *Front Cell Neurosci*. 2022;16:1025708. doi:10.3389/fncel.2022.1025708
19. Li W, Shen N, Kong L, et al. STING mediates microglial pyroptosis via interaction with NLRP3 in cerebral ischaemic stroke. *Stroke Vasc Neurol*. 2023:svn–2023–002320. doi:10.1136/svn-2023-002320.
20. McKenzie BA, Dixit VM, Power C. Fiery cell death: pyroptosis in the central nervous system. *Trends Neurosci*. 2020;43(1):55–73. doi:10.1016/j.tins.2019.11.005
21. Liu C, Yao K, Tian Q, et al. CXCR4-BTK axis mediate pyroptosis and lipid peroxidation in early brain injury after subarachnoid hemorrhage via NLRP3 inflammasome and NF-κB pathway. *Redox Biol*. 2023;68:102960. doi:10.1016/j.redox.2023.102960
22. Yang W, Chen W, Su H, et al. Recent advances in the development of histone deacylase SIRT2 inhibitors. *RSC Adv*. 2020;10(61):37382–37390. doi:10.1039/d0ra06316a
23. Harting K, Knöll B. SIRT2-mediated protein deacetylation: an emerging key regulator in brain physiology and pathology. *Eur J Cell Biol*. 2010;89(2–3):262–269. doi:10.1016/j.ejcb.2009.11.006
24. Sola-Sevilla N, Puerta E. SIRT2 as a potential new therapeutic target for Alzheimer's disease. *Neural Regen Res*. 2024;19(1):124–131. doi:10.4103/1673-5374.375315
25. She DT, Wong LJ, Baik S-H, Arumugam TV. SIRT2 inhibition confers neuroprotection by downregulation of FOXO3a and MAPK signaling pathways in ischemic stroke. *Mol Neurobiol*. 2018;55(12):9188–9203. doi:10.1007/s12035-018-1058-0
26. Shu L, Xu C-Q, Yan Z-Y, Yan Y, Jiang S-Z, Wang Y-R. Post-stroke microglia induce sirtuin2 expression to suppress the anti-inflammatory function of infiltrating regulatory T cells. *Inflammation*. 2019;42(6):1968–1979. doi:10.1007/s10753-019-01057-3
27. Yuan F, Xu Z-M, Lu L-Y, et al. SIRT2 inhibition exacerbates neuroinflammation and blood-brain barrier disruption in experimental traumatic brain injury by enhancing NF-κB p65 acetylation and activation. *J Neurochem*. 2016;136(3):581–593. doi:10.1111/jnc.13423
28. Chen H, Wu D, Ding X, Ying W. SIRT2 is required for lipopolysaccharide-induced activation of BV2 microglia. *Neuroreport*. 2015;26(2):88–93. doi:10.1097/WNR.0000000000000305
29. Xie XQ, Zhang P, Tian B, Chen XQ. Downregulation of NAD-dependent deacetylase SIRT2 protects mouse brain against ischemic stroke. *Mol Neurobiol*. 2017;54(9):7251–7261. doi:10.1007/s12035-016-0173-z
30. Wang W, Gong Q-Y, Cai L, et al. Knockout of Sirt2 alleviates traumatic brain injury in mice. *Neural Regen Res*. 2023;18(2):350–356. doi:10.4103/1673-5374.346457
31. Keskin-Aktan A, Akbulut KG, Abdi S, Akbulut H. SIRT2 and FOXO3a expressions in the cerebral cortex and hippocampus of young and aged male rats: antioxidant and anti-apoptotic effects of melatonin. *Biol Futur*. 2022;73(1):71–85. doi:10.1007/s42977-021-00102-3
32. Shen Z, Zhou H, Li A, et al. Metformin inhibits hepatocellular carcinoma development by inducing apoptosis and pyroptosis through regulating FOXO3. *Aging (Albany NY)*. 2021;13(18):22120–22133. doi:10.18632/aging.203464
33. Liu X-L, Gao -C-C, Qi M, Han Y-L, Zhou M-L, Zheng L-R. Expression of FOXO transcription factors in the brain following traumatic brain injury. *Neurosci Lett*. 2021;753:135882. doi:10.1016/j.neulet.2021.135882
34. Wang R, Liang Z, Xue X, et al. Microglial FoxO3a deficiency ameliorates ferroptosis-induced brain injury of intracerebral haemorrhage via regulating autophagy and heme oxygenase-1. *J Cell Mol Med*. 2024;28(1):e18007. doi:10.1111/jcmm.18007
35. Panni P, Simionato F, Cao R, et al. Hemorrhage volume drives early brain injury and outcome in poor-grade aneurysmal SAH. *AJNR Am J Neuroradiol*. 2024;45(4):393–399. doi:10.3174/ajnr.A8135
36. Gao -Y-Y, Tao T, Wu D, et al. MFG-E8 attenuates inflammation in subarachnoid hemorrhage by driving microglial M2 polarization. *Exp Neurol*. 2021;336:113532. doi:10.1016/j.expneurol.2020.113532
37. Chen -X-X, Tao T, Liu X-Z, et al. P38-DAPK1 axis regulated LC3-associated phagocytosis (LAP) of microglia in an in vitro subarachnoid hemorrhage model. *Cell Commun Signal*. 2023;21(1):175. doi:10.1186/s12964-023-01173-6
38. Chen X, He W-T, Hu L, et al. Pyroptosis is driven by non-selective gasdermin-D pore and its morphology is different from MLKL channel-mediated necroptosis. *Cell Res*. 2016;26(9):1007–1020. doi:10.1038/cr.2016.100
39. Zeyu Z, Yuanjian F, Cameron L, Sheng C. The role of immune inflammation in aneurysmal subarachnoid hemorrhage. *Exp Neurol*. 2021;336:113535. doi:10.1016/j.expneurol.2020.113535
40. Oladapo A, Jackson T, Menolascino J, Periyasamy P. Role of pyroptosis in the pathogenesis of various neurological diseases. *Brain Behav Immun*. 2024;117:428–446. doi:10.1016/j.bbi.2024.02.001
41. Omorou M, Huang Y, Gao M, et al. The forkhead box O3 (FOXO3): a key player in the regulation of ischemia and reperfusion injury. *Cell Mol Life Sci*. 2023;80(4):102. doi:10.1007/s00018-023-04755-2